SHORT COMMUNICATION

Proton Pathways and H^+/Cl^- Stoichiometry in Bacterial Chloride Transporters

Zhifeng Kuang, Uma Mahankali, and Thomas L. Beck*
Department of Chemistry, University of Cincinnati, Cincinnati, Ohio 45221-0172

ABSTRACT H^+/Cl^- antiport behavior has recently been observed in bacterial chloride channel homologs and eukaryotic CLC-family proteins. The detailed molecular-level mechanism driving the stoichiometric exchange is unknown. In the bacterial structure, experiments and modeling studies have identified two acidic residues, E148 and E203, as key sites along the proton pathway. The E148 residue is a major component of the fast gate, and it occupies a site crucial for both H^+ and Cl^- transport. E203 is located on the intracellular side of the protein; it is vital for H^+, but not Cl^-, transport. This suggests two independent ion transit pathways for H^+ and Cl^- on the intracellular side of the transporter. Previously, we utilized a new pore-searching algorithm, TransPath, to predict Cl^- and H^+ ion pathways in the bacterial ClC channel homolog, focusing on proton access from the extracellular solution. Here we employ the TransPath method and molecular dynamics simulations to explore H^+ pathways linking E148 and E203 in the presence of Cl^- ions located at the experimentally observed binding sites in the pore. A conclusion is that Cl^- ions are required at both the intracellular (S_{int}) and central (S_{cen}) binding sites in order to create an electrostatically favorable H^+ pathway linking E148 and E203; this electrostatic coupling is likely related to the observed $1H^+$/$2Cl^-$ stoichiometry of the antiporter. In addition, we suggest that a tyrosine residue side chain (Y445), located near the Cl^- ion binding site at S_{cen}, is involved in proton transport between E148 and E203. Proteins 2007;68:26–33. © 2007 Wiley-Liss, Inc.

Key words: electrostatics; ion channels; transporters; exchange mechanism

INTRODUCTION

The prediction of the double-barreled structure of chloride channels based on physiological measurements[1,2] was recently confirmed by the X-ray structure determination of bacterial CLC family homologs.[3] The observed homodimeric structure is complex, exhibiting an array of widely oriented α-helices that create an hourglass structure. The intracellular and extracellular vestibules are separated by a narrow 15 Å filter region. The filter is strongly electropositive.[4] The N-terminal domains of several of the helices, in an antiparallel arrangement, point toward the Cl^- ion pore so as to create the electropositive potential. The crystal structure includes anions bound at a central site in the filter, S_{cen}, and an internal site, S_{int}, near the intracellular entrance to the filter. A third binding site, S_{ext}, is occupied either by the gating residue E148 in the closed state or an anion when the gate is mutated and has moved to an open position.[5] For the open state, structural studies suggest that all three anion ion binding sites can be simultaneously occupied.[6]

Sequence alignment and homology modeling have led to helpful analogies between the prokaryotic and eukaryotic CLC proteins.[3,7–12] Recently, however, the initial view that the bacterial structure might provide direct understanding of eukaryotic chloride channel function was challenged by the discovery of stoichiometric $1H^+$/$2Cl^-$ exchange behavior in the bacterial homologs.[13] To further blur the boundaries between the chloride channels and antiporters, H^+/Cl^- exchange behavior has now been detected in the eukaryotic ClC-4 and ClC-5 family members.[14–16] Finally, functional importance of the chloride transporters has been demonstrated for nitrate accumulation in plant vacuoles.[17]

The accumulating experimental and modeling evidence indicates that channels like ClC-0 and transporters such as EcClC, ClC-4, and ClC-5 share many common features, but also contain targeted changes that convert the transporter into a channel.[18] The bacterial E148 gating residue is conserved throughout the entire family (except the ClC-K channel).[3] This residue is located near the

extracellular exit of the selectivity filter, and acts as a fast gate. Residues homologous to EcClC E203, however, appear only in the transporter class.[19] This suggests that E203 is crucial for proton transport, but not for chloride permeation. E203 is located toward the intracellular side of the protein, but is not fully exposed to the aqueous vestibule. Separate pathways for Cl$^-$ and H$^+$ motion were previously suggested based on our pore-searching algorithm, TransPath, which probes geometrically and electrostatically favorable pathways for ion motion through membrane proteins.[4] The possible importance of the E203 residue for proton motion across the transporter was noted, and experiments have shown that mutation of the E203 residue abolishes proton transport.[19]

In this Short Communication, we utilize the Trans-Path algorithm to explore possible proton pathways linking the two key acidic residues E148 and E203. We present the radius and electrostatic potential profiles for two possible pathways linking the E148 and E203 proton binding sites. The potential profile is also examined for four cases of chloride ion configurations in the pore: no chloride ions, one chloride ion at the internal binding site S_{int}, one chloride ion at the central binding site S_{cen}, and two chloride ions located at S_{cen} and S_{int}. We find that chloride ions are required at both binding sites to create an electronegative proton pathway linking E148 and E203. This electrostatic coupling may be a major factor determining the observed 1H$^+$/2Cl$^-$ stoichiometry of the transporter. In addition, a tyrosine residue (Y445), whose side chain is located near a chloride ion binding site (S_{cen}), is suggested to be involved in proton transport. Preliminary molecular dynamics simulations are also carried out to investigate E148 gate opening free energies. A possible exchange mechanism is outlined that is consistent with experiment, electrostatic modeling, and molecular dynamics simulations (see the Added Notes at the end).

METHODS

The prediction of ion permeation pathways can be attempted at various levels of detail. Molecular dynamics,[7,12,20–23] Brownian dynamics,[8,12] and Monte Carlo[24] simulation methods have been employed to study aspects of ion motion through chloride channels and their homologs. While these techniques provide a high level of molecular detail, they are limited by time and length scales due to the high computational overhead. In addition, even though theoretical techniques are available to model proton motion in water and through proteins, accurate dynamical modeling of proton motion presents an even higher level of computational complexity than standard molecular dynamics simulations.[25,26]

To examine possible proton pathways, here we employ a coarser-level description. Given the input of an X-ray crystal structure, we solve the Poisson equation at the continuum dielectric level using a multigrid numerical technique.[27] This potential is then used as input to our

search algorithm, TransPath.[4] This algorithm employs a biased Monte Carlo method to exhaustively sample possible ion permeation pathways through the protein structure. The penalty function in the searching contains terms which drive the sampling into regions of favorable geometry (open space) and electrostatic potential for ions of a given charge. We emphasize that explicit physical ions are not included in the modeling; rather, the algorithm searches for the cavity of maximum size once the guided trajectories have sampled electrostatically favorable domains. Trajectories that make their way out of the protein into the intracellular or extracellular spaces are saved and analyzed. Once successful exiting trajectories are located, the paths are optimized to maximize the available free space. The outputs of TransPath are path coordinates, radius profile, potential profile (the potential due to the protein), and pore-lining residues. Of course an infinity of paths are possible during the stochastic process of ion transport through the protein; this algorithm yields a guide as to the important domains. Further details can be found in Ref. 4 and in an article by Kuang Z, Liu A, and Beck TL (TransPath: a computational method to study the ion transit pathways in membrane channels, article in preparation).

The method is robust, and has been tested on several channels, including the gramicidin and potassium channels, in addition to the chloride transporter results presented here and elsewhere. Given a protein structure, the method consistently locates the same pathway or set of potential pathways for ions of a given charge. Placement of specific waters in a given pore can potentially block a given pathway during searching due to geometric effects; the purpose of this work is to explore electrostatically favorable regions, generated by the protein structure, for proton motion. Specific molecular aspects of proton motion through the transporter will be the subject of future work. The importance of electrostatic driving forces for proton motion through channels has been emphasized previously.[28,29]

For the searching process, we assumed dielectric constants of $\epsilon = 4$ for the protein and $\epsilon = 80$ for water. Protein partial charges were obtained from the CHARM22 force field.[30] An acidic residue near E203, E113, was neutralized based on previous electrostatics modeling of pK$_a$ shifts.[31] Using the TransPath method,[4] we searched for viable pathways for proton motion between the E148 and E203 residues. The closest distance between the E148 (OE1 carboxylate oxygen) and E203 (OE2 carboxylate oxygen) side chains in the crystal structure is 12.8 Å (Fig. 1). The z direction is taken as normal to the plane of the membrane. The z locations of several key sites are as follows: S_{int} ($z = -8.4$ Å), S_{cen} ($z = -2.8$ Å), S_{ext}/E148 (closed) ($z = 1.2$ Å), and E203 ($z = -9.0$ Å for the OE2 carboxylate oxygen). The TransPath searching was performed on the PDB 1OTS structure, which corresponds to the closed wild-type structure, and the E148 side chain was assumed charged during the searching. The initial TransPath searching was performed with no chloride ions in the pore; subsequently, the searching
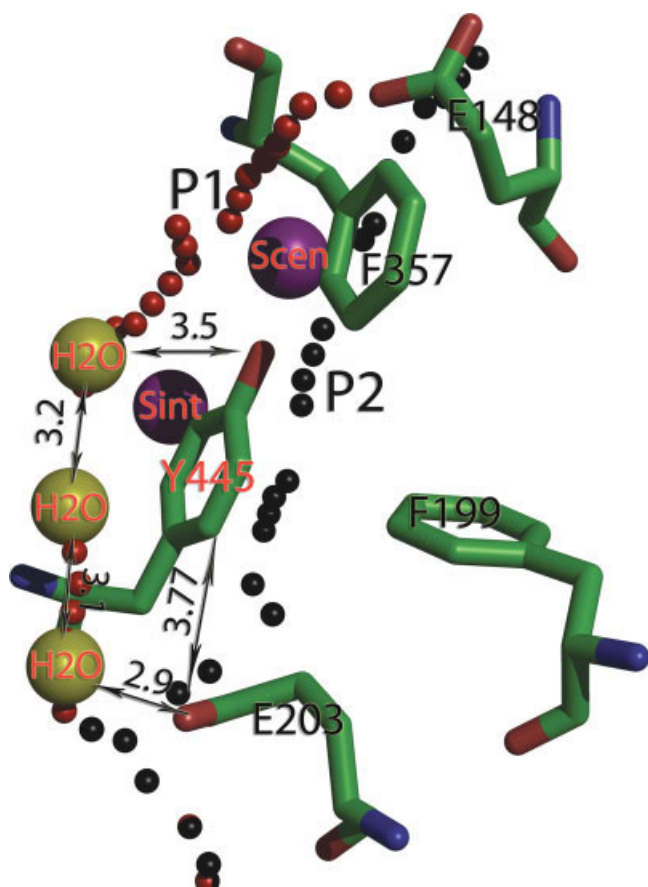
Fig. 1.   The two proton transit pathways (P1-dark red, P2-black). The S_{int} and S_{cen} binding sites are displayed; the third anion binding site at S_{ext} is located at the site occupied by the E148 side chain (closed configuration) in this figure. The paths are viewed from the dimer interface. Based on the radius profile of P1, three water molecules (tan spheres, $z = -8.8$ Å, $z = -6.3$ Å, and $z = -4.3$ Å) were placed in the pore. The water at $z = -8.8$ Å is resolved in the X-ray structure. The possible water wire is along the three displayed waters. Distances are indicated on the figure. The figure was generated with the PYMOL program.

was done with chloride ions at the S_{int} and S_{cen} sites, and the same two prototype pathways were found.

Molecular dynamics simulations were performed with the NAMD code[32] (CHARMM22 force field and TIP3P water model[30]). The X-ray structure (Protein Data Bank code: 1OTS) of the EcClC transporter reveals a dimer in a rhombus shape, with major and minor diagonals of 100 and 55 Å, respectively. The E148 side chain is located more than 15 Å from any membrane atoms; to reduce the computational cost, the membrane was thus replaced with a model rigid membrane of nonpolar atoms. The radius of these nonpolar atoms was set at 2.5 Å and the parameters for the nonbonded interactions were adjusted to prevent water penetration, and to generate a physically reasonable density of water molecules at the membrane–water interface. The protein-membrane system was immersed in a water box and 48 Na^+ and 58 Cl^- ions were added to neutralize the total charge and to

yield a net ion concentration of roughly 150 mM. Water molecules were added to protein cavities with the DOWSER program.[33] The initial EcClC protein system was minimized for 1500 steps and then equilibrated for 200 ps with the protein fixed, followed by 5 ns equilibration with the protein free to move. The protonated E148 residue was generated following the equilibration period. A timestep of 2 fs was employed, Langevin dynamics was used to maintain a temperature of 300 K, and the particle-mesh-Ewald algorithm[34] was utilized for the long-ranged electrostatic interactions. All missing atoms of the resolved residues in the structure were added with CHARMM utilities.[30] The missing residues in the termini of the structure were not reconstructed since they reside in the cytoplasmic solution far from the interesting pore region.

The free energy profile for gate opening was calculated using the Adaptive Biasing Force method[35] in the NAMD code.[32] The dihedral angle CA-CB-CG-CD (starting with the α-carbon of the E148 side chain) was the chosen coordinate for the opening process. The dihedral angle was sampled through a 160° range in windows of 5°. Each angular window was sampled for 150 ps.

RESULTS

Two prototype proton pathways were located in the regions connecting the E148 and E203 residues, here labeled P1 and P2. Figure 1 displays the pathways, viewed from the dimer interface of the EcClC (1OTS) structure to enhance the visualization. We will describe the pathways proceeding from the negative z regions near E203 to the oxygen atoms of the E148 carboxylate, which are at slightly positive z values. This orientation is assumed here to conform to the orientation of the figures. As will be seen in the radius profile below, the P1 path near the E203 residue has a radius large enough to accommodate up to three water molecules. The first water at the bottom of Figure 1 appears in the crystal structure, and we have labeled two other possible water binding sites along the path. After leaving the location of the third water molecule shown in Figure 1, the P1 path then continues through the protein, ending some distance from the E148 gate. Therefore, we conclude the upper portion of this pathway is likely not involved in proton transport. The other located path, P2, proceeds from E203 directly along the aromatic ring of the Y445 side chain, past the Y445 OH group, and toward the S_{cen} chloride ion binding site. Y445, along with S107, binds a chloride ion at the S_{cen} site in the crystal structure. The path passes very near the S_{cen} chloride ion location, and then heads directly toward the E148 oxygens along the chloride ion pore. Besides the S107 and Y445 residues, the pathways are devoid of possible protein hydrogen-bonded-chain sites for protons as they pass between E148 and E203.

Figure 2(a) displays the radius profiles for the P1 and P2 proton paths. As discussed above, the P1 path exhibits a larger radius profile in the low-z regions compared
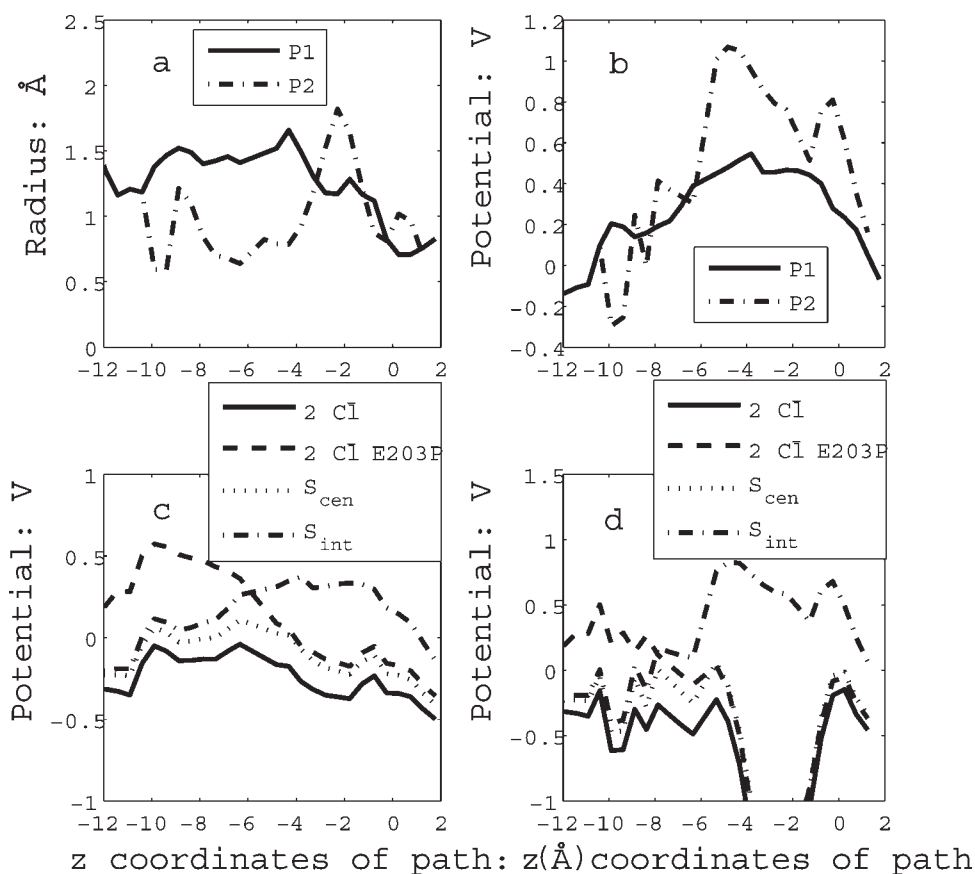
Fig. 2.   (**a**) The radius profiles for the P1 and P2 paths. (**b**) The potential profiles for the P1 and P2 paths in the absence of anions in the pore. (**c**) The potential profiles for P1 path for the cases: one anion at S_{int}, one anion at S_{cen}, anions at both S_{int} and S_{cen} with E203 protonated, and anions at both S_{int} and S_{cen} with E203 unprotonated. (**d**) The potential profiles for the P2 path for the cases: one anion at S_{int}, one anion at S_{cen}, anions at both S_{int} and S_{cen} with E203 protonated, and anions at both S_{int} and S_{cen} with E203 unprotonated. The z locations of key sites are as follows: $z(S_{cen}) = -2.8$ Å, $z(S_{int}) = -8.4$ Å, $z(\text{E203-OE2}) = -9.0$ Å, and $z(\text{E148-OE1}) = 1.2$ Å.

with the P2 path. The crystal water displayed in Figure 1 is located at $z = -8.8$ Å, and the radius profile is large enough to possibly accommodate two more water molecules, at $z = -6.3$ and -4.3 Å locations, before a reduction in pore radius occurs. The three potential water locations discussed here appear as small peaks in the radius profile. The P2 path exhibits a significantly smaller radius between $z = -10$ and $z = -4$ Å, except for a peak at roughly $z = -8.5$ Å. That location may also potentially accommodate a water molecule. The large peak in the radius profile of the P2 path between $z = -2$ and $z = -3$ Å is due to the chloride ion at the S_{cen} binding site in the crystal structure.

The potential profiles in the absence of any chloride ions in the filter are displayed in Figure 2(b). Both profiles exhibit large positive barriers to proton propagation between E148 and E203. This implies that protons will not move between E148 and E203 in the absence of chloride ions in the pore. Figure 2(c,d) displays the potential profiles for the P1 [Fig. 2(c)] and P2 [Fig. 2(d)] paths in the presence of chloride ions in the filter region. It is

clear from both potential profiles that, for the $z < -5$ Å region, chloride ions are required at the S_{int} and S_{cen} binding sites to create an electronegative potential. Also, the S_{cen} chloride ion has a larger effect on the potential profile than the S_{int} chloride ion. The very large, negative potential centered at $z = -3$ Å in Figure 2(d) is due to the chloride ion at the S_{cen} binding site. In addition, we plot the potential profile for the case where the E203 residue is protonated, and a large positive lobe appears near $z = -9$ to -10 Å, indicating that a proton would be repelled from the region around E203 should that residue be protonated.

Further TransPath calculations were performed to examine the impact of protonation of the E148 gate on the anion energetics through the pore. In Figure 3, we show the computed potential profiles along the anion pathway for the unprotonated and protonated states of the closed E148 gate (the anion electrostatic energy due to the protein potential is minus the values shown). Figure 3(a) displays the two potential profiles with the S_{int} site empty. It is clear that protonation of the E148 gate
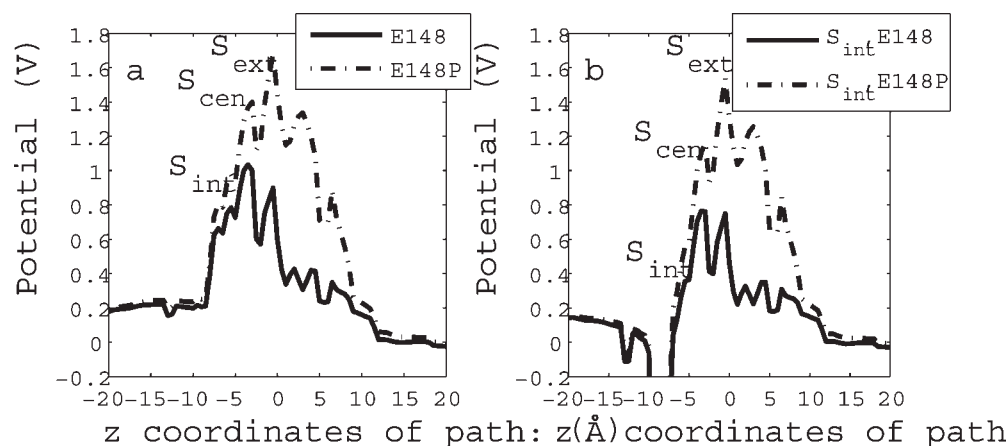
Fig. 3.   Potentials profiles along the anion pathway: (**a**) potential profiles with no anions in the pore. The top dashed curve is for the protonated E148 gate, and the bottom solid curve is for the unprotonated E148 gate. The electrostatic barrier faced by an anion sitting at the S_{cen} binding site moving toward the S_{ext} site is roughly 5.6 kcal/mol for the protonated E148 case, and 10 kcal/mol for the unprotonated E148 gate. (**b**) potential profiles with a chloride ion located at the S_{int} binding site. The top dashed curve is for the protonated E148 gate, and the bottom solid curve is for the unprotonated E148 gate. The electrostatic barrier faced by an anion sitting at the S_{cen} binding site moving toward the S_{ext} site is roughly 3.9 kcal/mol for the protonated E148 case, and 8.3 kcal/mol for the unprotonated E148 gate.

leads to a more favorable potential for the anion located at S_{cen}. Also, the electrostatic barrier for anion motion from the S_{cen} site toward S_{ext} site is reduced from roughly 10 kcal/mol to 5.6 kcal/mol upon protonation. In Figure 3(b), the potential profiles for the unprotonated and protonated E148 cases are presented in the presence of a chloride ion at the S_{int} binding site. The electrostatic barrier for motion of an ion at S_{cen} moving toward S_{ext} is 8.3 kcal/mol for the unprotonated E148 case and reduced to 3.9 kcal/mol when the gate is protonated. The corresponding potential profiles for the E148Q (open) mutant are presented in our previous article.[4] These results from simple electrostatics calculations are consistent with recent molecular dynamics simulations,[21,23] which implicate an ion-push-ion reduction in the free energy barrier for anion permeation.

In related work, we have utilized molecular dynamics simulations to compute the free energy profile for opening of the E148 gate in both the protonated and unprotonated forms, and in the absence of the ion-push-ion force discussed above (the S_{int} site was unoccupied and the S_{cen} site was occupied for this initial simulation; Mahankali U, Beck TL. Free energy profiles for fast gate opening in bacterial ClC transporters, in preparation). A free energy profile with roughly a 10 kcal/mol barrier for rotation of the E148 dihedral angle toward the open state was calculated for the protonated form, with a 5 kcal/mol increase in the barrier for the unprotonated form. Only a very shallow well was observed for the open conformation. This finding is consistent with the discussion of Lobet and Dutzler,[6] who noted that it has not been possible to obtain a crystal structure for the open state in the wild-type EcClC transporter; they suggested that the open state may not exhibit a deep free energy minimum. We are currently examining the gate

opening free energy profile with both S_{int} and S_{cen} sites occupied with chloride ions to probe the impact of the S_{int} ion via the ion-push-ion effect. This presumably lowers the free energy barrier for gate opening by exertion of an asymmetric force on the E148 side chain.[21] These results, along with the electrostatic modeling, indicate that protonation of the E148 gate stimulates opening and conduction of anions through the pore on relatively rapid time scales.

DISCUSSION

Based on the TransPath searching results, we located two possible pathways for proton propagation between E148 and E203. Both of these pathways require chloride ion occupancy at the S_{int} and S_{cen} binding sites to create an electronegative conduit between the E148 and E203 residues. The S_{cen} anion has a more dominant effect on the potential profile than the S_{int} anion. We suggest that this electrostatic coupling provides a clue to the stoichiometry of the transporter. In the following discussion, we will assume that the proton starts from the protonated state of the E148 residue and proceeds to propagate toward the E203 residue. The transporter functions in both directions.[13]

The most likely pathway leaving the E148 residue is the P2 path that heads directly toward the S_{cen} binding site. Because of the strong positive potential in the filter region, the S_{cen} binding site has a high probability of chloride ion occupancy, and the proton will be strongly attracted in the direction of S_{cen} once that site is occupied [Fig. 2(d)]. At this point, the TransPath searching suggests either of two possible pathways. The first, along P1, consists of a water wire located near and perhaps oriented by the Y445 residue, and the second, P2, moves

in a "shortcut" alongside Y445, interacting directly with the OH group and the aromatic ring. Experiments have shown the involvement of tyrosine residues in proton propagation through proteins,[36,37] and calculations also imply a strong interaction.[38,39] Those quantum chemical models[39] indicate the possible strong binding of protons to the aromatic ring of the tyrosine side chain. The proton affinity of a single water molecule is −160 kcal/mol (for a water dimer, the value is about 20% larger in magnitude, or roughly −190 kcal/mol),[40] while the proton affinity of a tyrosine OH group is calculated to be −197 kcal/mol, and the values for binding to the aromatic ring range between −187 and −209 kcal/mol.[38]

Since both of the pathways pass near the Y445 residue, we thus propose that Y445 is an important participant in proton propagation. This residue has been mutated in physiological studies of eukaryotic chloride channels,[41,42] but not in the bacterial[19] or eukaryotic ClC-4,5 transporters (see Added Notes at the end).[14,15] For the channels, mutation of the Y445 homolog had little effect on chloride ion transport. Our proposal here is that this residue, while not essential for chloride ion propagation, may be crucial for proton movement through the protein.

Although many possible scenarios could be imagined to rationalize the transporter mechanism, we suggest a sequence of steps that is consistent with experiment, previous modeling and simulations, and the results presented here. The net movement is of two chloride ions from the pore into the extracellular space, and one proton from the E148 gate to the intracellular region, including a stop at the E203 residue.

The initial step in this model is protonation of the E148 gate in the closed configuration. The E148 gate open probability is strongly dependent on pH in ClC channels,[43] and mutation of this residue abolishes proton activity in the transporters.[19] In the closed state and in the absence of nearby chloride ions, the pK_a shift of the E148 residue is large and negative.[44] The prediction of protonation equilibrium for this residue is highly sensitive to the assumed protein dielectric constant in continuum models, but it is clear from those previous calculations that chloride ions in close proximity to E148 are required to shift the pK_a into the experimentally observed range. Electrostatics calculations[4,31] and molecular dynamics simulations[23] indicate a relatively weak chloride ion binding site, S_{bs}, on the extracellular side of the E148 gate. The electrostatic well is created by the R147 residue (and perhaps other basic residues[31]) situated just outside the entrance to the pore. An S_{bs} anion is not observed in the crystal structures,[6] but this would not be expected since it is located in the aqueous vestibule. The other nearby chloride ion occupies the S_{cen} binding site, roughly 4 Å from the E148 side chain. These previous protonation calculations thus suggest that such a "chloride sandwich" configuration is necessary to stimulate protonation of E148.

As discussed above, electrostatics calculations and molecular dynamics simulations of the gating process indicate that, if the E148 gate is protonated, the barrier to

gate opening is not large, and it thus opens on a fairly rapid time scale. The barrier to anion permeation, once the gate is protonated, is on the order of only 4 kcal/mol, and thus the chloride ion at S_{cen} moves toward the slightly more stable S_{ext} position. While the S_{ext} site is occupied, the gate will stay open and protonated due to the close proximity of chloride ions. This is the chloride conduction stage of the proposed mechanism, and X-ray crystallography studies[6] on mutant transporters indicate the pore can be simultaneously occupied with up to 3 anions (at S_{int}, S_{cen}, and S_{ext}; there is no corresponding structure for the wild-type transporter, however). On average, two chloride ions exit the pore, those initially located at S_{int} and S_{cen}. Because of the apparent downhill free energy profile for the protonated E148 gate closing, vacancy of the S_{ext} site leads to gate closing.

In our model, the next step in the exchange cycle is release of the proton from E148 at the S_{ext} site. Presumably the S_{int} and S_{cen} sites refill with chloride ions from the intracellular solution at some point during the chloride conduction phase. The chloride ion at the S_{cen} binding site creates a strong electrostatic attraction for the proton as it leaves the E148 residue [Fig. 2(d)]. Since we rationalized the *protonation* of the E148 side chain based on S_{cen} (and S_{bs}) occupancy, this may seem like a contradiction. The experimentally estimated pK_a of the E148 homolog in a ClC channel[43] is, however, roughly 5.3, so it is likely the chloride ion occupancy merely shifts the E148 pK_a into a range into one which allows for relatively frequent protonation/deprotonation events. As the proton is released and approaches the S_{cen} chloride ion, it is then also in the vicinity of the S107 and Y445 residues. Since mutation of the Y445 homolog in chloride channels has only a minor effect on anion conductance, we suggest that an important role of the Y445 residue is to mediate proton propagation either through stabilizing a proton wire (P1) or through a direct interaction with the aromatic ring (P2). The persistence of the Y445 homolog in eukaryotic channels may be an evolutionary remnant along the lines of the 'degraded transporter' picture of Miller.[18] Along these lines, we also note the relatively close proximity of the F357 side chain to the P2 path, between the S_{ext} and S_{cen} binding sites.

The proton then proceeds to the E203 side chain along a path made electrostatically favorable by the chloride ions occupying the S_{int} and S_{cen} binding sites. As discussed above, there appear to be two possible pathways, one along a water wire that may be oriented by the Y445 side chain, and one interacting more directly with the aromatic ring. The final step of this proposed cycle is release of the proton from the E203 residue. This release is likely linked either to one of two causes: depletion of chloride ions from the S_{int} and S_{cen} sites at the beginning of the next transport cycle (leading to a pK_a shift of the E203 side chain), or to the formation of a salt bridge of E203 with a basic residue. Accardi and Miller[19] found that mutation of R28 (from the other monomer) did not abolish proton transport, but we have observed motion of the K216 residue (also from the other monomer) into

close proximity of the E203 residue during molecular dynamics simulations.

CONCLUSIONS

This paper has presented modeling studies of the bacterial chloride transporter, aimed at gaining a glimpse at the mechanism of proton/chloride antiport. Two main conclusions follow from the electrostatic picture presented here. First, passage of a proton between the E148 and E203 residues is intimately coupled with chloride ion occupancy at the S_{int} and S_{cen} binding sites in the pore, with the S_{cen} ion playing a more prominent role. Second, two possible proton paths located utilizing the TransPath algorithm both pass near the Y445 side chain, which is located near the S_{cen} binding site. Mutation of this side chain does not significantly alter chloride ion conduction in eukaryotic channels, and we propose that Y445 is a residue along the proton path in a manner consistent with other discussions of the role of tyrosine in proton propagation through proteins.[36,37] Since there are no other hydrogen-bonding residue side chains (besides S107) in the vicinity of the predicted proton paths, we suggest the Y445 residue itself and/or a possible water wire next to Y445 are important for proton migration between E148 and E203.

Future work will focus on detailed molecular dynamics and quantum chemical studies of the free energy (and protonation equilibrium) characteristics of each of the steps in the mechanism proposed above. Efficient methods for calculating the *absolute* hydration free energies for ions in solution have been developed recently (Feng G, Beck TL, Pratt LR. Efficient and accurate computations of electrostatic contributions to solvation free energies, in preparation);[45] these methods utilize the Potential Distribution Theorem (PDT) expression for the chemical potential. That expression includes contributions to the total chemical potential from the ideal (density dependent) term, an excess (chemical) part, and an external field. The methods developed in our group allow for the computation of the excess part in a single (or at most a few) simulations, which reduces the overall cost relative to, for example, thermodynamic integration. The PDT approach yields a local description of the excess chemical potential, which allows for computation of the solvation free energy of an ion (or molecular solute generally) at any position in space. Thus potentials of mean force (PMFs) can be readily obtained. In addition, the free energy can be exactly partitioned into van der Waals and electrostatic contributions, which can produce helpful insights into the separate driving forces for ion transport. Given a standard modern force field representation, this partitioning can be viewed as first inserting a van der Waals particle, and then "turning on" the charges; we have developed separate methods for the van der Waals and electrostatics parts of the free energy.

Computations of accurate anion free energies are complicated by the large polarizabilities, which may not be accurately modeled with standard force fields;[46–48]

for example, the polarizabilities can lead to quite different solvation free energies and surface activities for chloride and bromide ions. Finally, direct simulation of proton motion through the transporter utilizing Empirical Valence Bond (EVB) theory is a feasible option.[25,26] Further experiments and these computational and theoretical tools should help to provide a more detailed picture of proton motion through the fascinating H^+/Cl^- transporters.

Added notes: Just prior to completion of this article, we became aware of a forthcoming experimental paper by Accardi et al.[49] in which the Y445 residue was mutated and the EcClC function examined. It is clear from that work that the hydroxyl group of Y445 is not crucial for proton motion through the exchanger. The mutations Y445F and Y445W preserve the H^+/Cl^- exchange behavior of the transporter, and this may indicate an important function for the aromatic ring. [Computationally enacting the Y445F mutation led to only very minor changes in the radius and potential profiles corresponding to Figure 2(a,b) (data not shown). This shows that the basic path structure and potential profiles do not change substantially with the mutation.] The authors did note that it is possible that a water molecule might potentially substitute at the Y445 OH site in the mutants (although no water was resolvable at that site in the X-ray structure). Ref. 49 emphasizes the important role of S_{cen} anion occupancy for proton motion through the exchanger. The specific role of Y445 and its mutants in anion binding at S_{cen} is unknown, but should be the subject of future experiments and molecular-level simulations. The present work was presented at the Telluride workshop on Epithelial Physiology and Cell Biology on July 24, 2006.

REFERENCES

1. Miller C, White MM. Dimeric structure of single chloride channels from Torpedo electroplax. Proc Natl Acad Sci USA 1984;81:2772–2775.
2. Middleton RE, Pheasant DJ, Miller C. Purification, reconstitution, and subunit composition of a voltage-gated chloride channel from Torpedo electroplax. Biochemistry 1994;33:13189–13198.
3. Dutzler R, Campbell EB, Cadene M, Chait BT, MacKinnon R. X-ray structure of a ClC chloride channel at 3.0 A reveals the molecular basis of anion selectivity. Nature 2002;415:287–294.
4. Yin J, Kuang Z, Mahankali U, Beck TL. Ion transit pathways and gating in ClC chloride channels. Proteins 2004;57:414–421.
5. Dutzler R, Campbell EB, MacKinnon R. Gating the selectivity filter in ClC chloride channels. Science 2003;300:108–112.
6. Lobet S, Dutzler R. Ion-binding properties of the ClC chloride selectivity filter. EMBO J 2006;25:24–33.
7. Moran O, Traverso S, Elia L, Pusch M. Molecular modeling of *p*-chlorophenoxyacetic acid binding to the CLC-0 channel. Biochemistry 2003;42:5176–5185.

8. Corry B, O'Mara M, Chung SH. Conduction mechanisms of chloride ions in ClC-type channels. Biophys J 2004;86:846–860.

9. Chen TY. Structure and function of CLC channels. Annu Rev Physiol 2005;67:809–839.

10. Dutzler R. The ClC family of chloride channels and transporters. Curr Opin Struct Biol 2006;16:439–446.

11. Jentsch TJ, Poet M, Fuhrmann JC, Zdebik AA. Physiological functions of CLC Cl$^-$ channels gleaned from human genetic disease and mouse models. Annu Rev Physiol 2005;67:779–807.

12. Bisset D, Corry B, Chung SH. The fast gating mechanism in ClC-0 channels. Biophys J 2005;89:179–186.

13. Accardi A, Miller C. Secondary active transport mediated by a prokaryotic homologue of ClC Cl$^-$ channels. Nature 2004;427:803–807.

14. Picollo A, Pusch M. Chloride/proton antiporter activity of mammalian CLC proteins ClC-4 and ClC-5. Nature 2005;436:420–423.

15. Scheel O, Zdebik AA, Lourdel S, Jentsch TJ. Voltage-dependent electrogenic chloride/proton exchange by endosomal CLC proteins. Nature 2005;436:424–427.

16. Pusch M, Zifarelli G, Murgia AR, Picollo A, Babini E. Channel or transporter? The CLC saga continues. Exp Physiol 2006;91:149–152.

17. De Angeli A, Monachello D, Ephritikhine G, Frachisse JM, Thomine S, Gambale F, Barbier-Brygoo H. The nitrate/proton antiporter AtCLCa mediates nitrate accumulation in plant vacuoles. Nature 2006;442:939–942.

18. Miller C. ClC chloride channels viewed through a transporter lens. Nature 2006;440:484–489.

19. Accardi A, Walden M, Nguitragool W, Jayaram H, Williams C, Miller C. Separate ion pathways in a Cl$^-$/H$^+$ exchanger. J Gen Physiol 2005;126:563–570.

20. Cohen J, Schulten K. Mechanism of anionic conduction across ClC. Biophys J 2004;86:836–845.

21. Gervasio FL, Parrinello M, Ceccarelli M, Klein ML. Exploring the gating mechanism in the ClC chloride channel via metadynamics. J Mol Biol 2006;361:390–398.

22. Suenaga A, Yeh JZ, Taiji M, Toyama A, Takeuchi H, Son M, Takayama K, Iwamoto M, Sato I, Narahashi T, Konagaya A, Goto K. Bead-like passage of chloride ions through ClC chloride channels. Biophys Chem 2006;120:36–43.

23. Bostick DL, Berkowitz ML. Exterior site occupancy infers chloride-induced proton gating in a prokaryotic homolog of the ClC chloride channel. Biophys J 2004;87:1686–1696.

24. Miloshevsky GV, Jordan PC. Anion pathway and potential energy profiles along curvilinear bacterial ClC Cl$^-$ pores: electrostatic effects of charged residues. Biophys J 2004;86:825–835.

25. Braun-Sand S, Burykin A, Chu ZT, Warshel A. Realistic simulations of proton transport along the gramicidin channel: demonstrating the importance of solvation effects. J Phys Chem B Condens Matter Mater Surf Interfaces Biophys 2005;109:583–592.

26. Voth GA. Computer simulation of proton solvation and transport in aqueous and biomolecular systems. Acc Chem Res 2006;39:143–150.

27. Beck TL. Real-space mesh techniques in density functional theory. Rev Mod Phys 2000;72:1041–1080.

28. Burykin A, Warshel A. What really prevents proton transport through aquaporin? Charge self-energy versus proton wire proposals. Biophys J 2003;85:3696–3706.

29. Chen H, Wu Y, Voth GA. Origins of proton transport behavior from selectivity domain mutations of the aquaporin-1 channel. Biophys J 2006;90:L73–L75.

30. Brooks BR, Bruccoleri RE, Olafson BD, States DJ, Swaminathan S, Karplus M. CHARMM: a program for macromolecular energy, minimization, and dynamics calculations. J Comput Chem 1983;4:187–217.

31. Faraldo-Gomez JD, Roux B. Electrostatics of ion stabilization in a ClC chloride channel homologue from Escherichia coli. J Mol Biol 2004;339:981–1000.

32. Kale L, Skeel R, Bhandarkar M, Brunner R, Gursoy A, Krawetz N, Phillips J, Shinozaki A, Varadarajan K, Schulten K. NAMD2: greater scalability for parallel molecular dynamics. J Comput Phys 1999;151:283–312.

33. Zhang L, Hermans J. Hydrophilicity of cavities in proteins. Proteins 1996;24:433–438.

34. Darden TA, York DM, Pedersen LG. An Nlog(N) method for Ewald sums in large systems. J Chem Phys 1993;98:10089–10092.

35. Henin J, Chipot C. Overcoming free energy barriers using unconstrained molecular dynamics simulations. J Chem Phys 2004;121:2904–2914.

36. Decoursey TE. Voltage-gated proton channels and other proton transfer pathways. Physiol Rev 2003;83:475–579.

37. Rotem D, Steiner-Mordoch S, Schuldiner S. Identification of tyrosine residues critical for the function of an ion-coupled multidrug transporter. J Biol Chem 2006;281:18715–18722.

38. Reddy AS, Sastry GN. Cation [M = H$^+$, Li$^+$, Na$^+$, K$^+$, Ca^{2+}, Mg^{2+}, NH$_4^+$, and NMe$_4^+$] interactions with the aromatic motifs of naturally occurring amino acids: a theoretical study. J Phys Chem 2005;109:8893–8903.

39. Dougherty DA. Cation-pi interactions in chemistry and biology: a new view of benzene, Phe, Tyr, and Trp. Science 1996;271:163–168.

40. Cheng H-P, Barnett RN, Landman U. All quantum simulations: H$_3$O(+) and H$_5$O$_2$(+). Chem Phys Lett 1995;237:161–170.

41. Estevez R, Schroeder BC, Accardi A, Jentsch TJ, Pusch M. Conservation of chloride channel structure revealed by an inhibitor binding site in ClC-1. Neuron 2003;38:47–59.

42. Chen MF, Chen TY. Side-chain charge effects and conductance determinants in the pore of ClC-0 chloride channels. J Gen Physiol 2003;122:133–145.

43. Chen MF, Chen TY. Different fast-gate regulation by external Cl(−) and H(+) of the muscle-type ClC chloride channels. J Gen Physiol 2001;118:23–32.

44. Beck TL, Yin J, Kuang Z, Mahankali U, Feng G. Comment on ion transit pathways and gating in ClC chloride channels. Proteins 2006;62:553–554.

45. Beck TL, Paulaitis ME, Pratt LR. The potential distribution theorem and models of molecular solutions. Cambridge: Cambridge University Press; 2006.

46. Bostrom M, Williams DR, Stewart PR, Ninham BW. Hofmeister effects in membrane biology: the role of ionic dispersion potentials. Phys Rev 2003;68(4, Part 1):041902.

47. Mucha M, Frigato T, Levering LM, Allen HC, Tobias DJ, Dang LX, Jungwirth P. Unified molecular picture of the surfaces of aqueous acid, base, and salt solutions. J Phys Chem B Condens Matter Mater Surf Interfaces Biophys 2005;109:7617–7623.

48. Ahn-Ercan G, Krienke H, Kunz W. Role of polarizability in molecular interactions in ion solvation. Curr Opin Colloid Interface Sci 2004;9:92–96.

49. Accardi A, Lobet S, Williams C, Miller C, Dutzler R. Synergism between halide binding and proton transport in a CLC-type exchanger. J Mol Biol 2006;362:691–699.